LUND UNIVERSITY

Patch antennas on inhomogeneous substrates

Rylander, Thomas; Abdelmassih Waller, Peter

2002

Patch antennas on inhomogeneous substrates

Thomas Rylander and Peter Waller

Thomas Rylander

Department of Electromagnetics
Chalmers University of Technology
SE-412 96 Göteborg
Sweden

Peter Waller

Department of Electroscience
Electromagnetic Theory
Lund Institute of Technology
P.O. Box 118
SE-221 00 Lund
Sweden

Abstract

Patch antennas on inhomogeneous substrates are analyzed with the stable FEM-FDTD hybrid method [T. Rylander and A. Bondeson, "Stable FEM-FDTD hybrid method for Maxwell's equations," *Comput. Phys. Comm.* **125**, 75 (2000)] and an analytic propagator technique. For inhomogeneous substrates with a *fixed homogenized value* of the permittivity, our results conjecture that a decrease of the permittivity in the vicinity of the patch increases the bandwidth and the resonance frequency. Furthermore, we find that inhomogeneous substrates with the permittivity only varying with the height influence the field pattern within the substrate, but not the radiation efficiency. The radiation patterns are computed with an FDTD program. However, only small influences on the radiation patterns are observed.

1   Introduction

Patch antennas are attractive in many applications since they are low-profile, cheap, mechanically robust, and simple to manufacture. However, the traditional patch antenna suffers from, *e.g.*, low efficiency and narrow frequency bandwidth. Thus, improved patch antenna designs have been pursued for many years. One part of the antenna that can be optimized is the substrate [1]. This can be done by designing different regions with constant permittivity [10]. Recently, Vegni *et al.* [17, 18] have proposed an inhomogeneous substrate with the permittivity continuously varying with the height coordinate. Improved bandwidth and directivity were reported. This problem has also been investigated in [9] under the assumption of a fixed current distribution on the patch. It was shown that the permittivity profile has much influence on the field pattern inside the substrate, but only a slight influence on the radiation pattern and efficiency.

In the present work, we optimize such antennas for large bandwidth operation using numerical computations and compare with recent analytical results. For the numerical computations, we use the stable hybrid method [14] which combines the Finite-Difference Time-Domain (FDTD) scheme and the Finite Element Method (FEM). It can handle a complex geometry without resorting to the staircase approximation, and the small structures of the coaxial cable feed are discretized by FEM. The rest of the computational domain, including the major part of the inhomogeneous substrate, is treated by the FDTD scheme. The time-step is set by the Courant condition of the FDTD, and it is not limited by the small cells needed to resolve the geometry of the feed. We also use an analytical technique [9] that assumes a given current distribution on the patch and an infinite substrate with a permittivity depending only on the height from the ground plane.
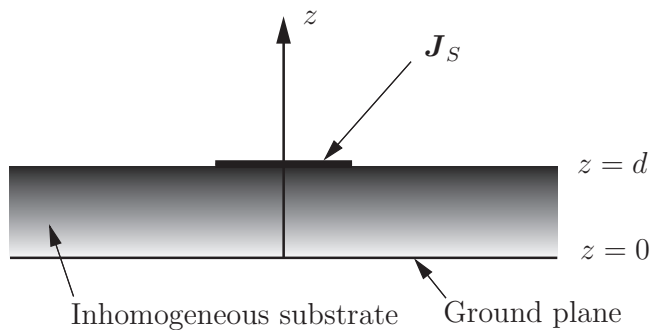
Figure 1: Geometry of the simulated structure, $\boldsymbol{J}_S$ is the given surface current density.

2 Methods for analysis

2.1 Analytical model

The analytical model, which treats the time harmonic case, is carefully described in [9]. The model is based on the assumption that we have an infinite substrate and an infinite ground plane. Thus, it is possible to Fourier transform the fields in the lateral directions (the x- and y-directions). The computation of the fields leads to a system of ordinary differential equations in the height coordinate (z-coordinate), see Figure 1. This approach can treat bianisotropic materials [11] and can also be extended to a MoM approach, *e.g.*, [8, 18].

A circular or rectangular patch is modeled using a given current placed above the substrate, corresponding to the dominant mode of the cavity model. The resonance frequency can be calculated according to the cavity model (without taking the fringing fields into account [2]), *i.e.*

$$
f_r = \begin{cases} \dfrac{1.841 c_0}{2\pi a \sqrt{\epsilon^{hom}}} & \text{Circular patch} \\[2ex] \dfrac{c_o}{2b\sqrt{\epsilon^{hom}}} & \text{Rectangular patch} \end{cases}
\tag{2.1}
$$

where a is the radius of the circular patch and b is the resonant length of the rectangular patch. The relative permittivity ϵ^{hom} is the homogenized value of the relative permittivity function $\epsilon(z)$, given by

$$
\frac{d}{\epsilon^{hom}} = \int\limits_0^d \frac{1}{\epsilon(z)}\mathrm{d}z,
\tag{2.2}
$$

where d is the thickness of the substrate. Here, $z = 0$ at the ground plane and $z = d$ at the air-dielectric interface. The electromagnetic fields inside and outside the substrate are solved using propagators [9] with the boundary conditions given by the Perfect Electric Conductor (PEC) ground plane and the radiation condition. We use a wave splitting technique [13] to impose the radiation boundary condition.
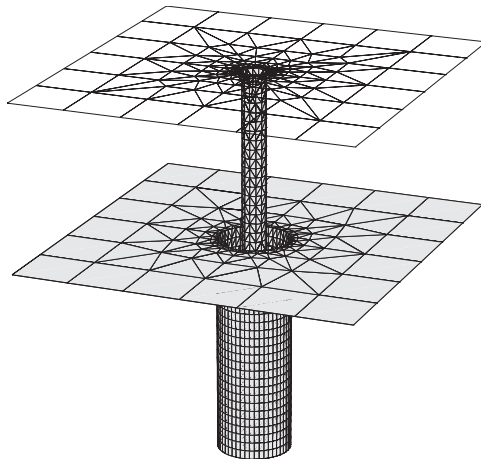
Figure 2: Finite element discretization of the coaxial cable feed.

2.2 Stable FEM-FDTD hybrid method

A patch antenna on an infinite substrate and an infinite ground plane can also be analyzed by the stable FEM-FDTD hybrid method [14]. Furthermore, the hybrid method can treat a finite substrate and/or a finite ground plane. Here, we feed the antenna by a coaxial cable with the relative permittivity $\epsilon = 1.86$, inner radius 0.48 mm, and outer radius 1.5 mm. The FEM is used in the vicinity of the feed point and parts of a typical grid are shown in Figure 2.

The geometry for our test case involving finite substrate and finite ground plane is shown in Figure 3, where the dimensions of the patch are kept fixed when the substrate and the ground plane are extended to infinity.

For computational reasons, the antenna is enclosed in an appropriate metal box. The walls of the box are covered by a so called sponge layer [12] which absorbs outward propagating waves. The antenna is driven by the TEM-mode launched from a port terminating the coaxial cable. Here, the launched wave has the time dependence

$$E_i(t) = E_0 \exp\left[-\left(\frac{t - t_0}{d_0} \right)^2 \right] \sin(2\pi f_0 (t - t_0)), \qquad (2.3)$$

where $f_0 = 2$ GHz, $d_0 = 2/(3f_0)$ and $t_0 = 3/f_0$. The time dependence of the reflected wave $E_r(t)$ is recorded at the port and the reflection coefficient is $S_{11}(f) = E_r(f)/E_i(f)$. The radiation pattern can be calculated by means of the near-to-far-field transformation [16].

In order to treat inhomogeneous materials, the hybrid code has been extended with numerical integration [5, 6, 20] for the finite elements. We use the portable, extensible toolkit for scientific computation (PETSc) [3] for the solution of the linear system of equations associated with the FEM part of the computations.
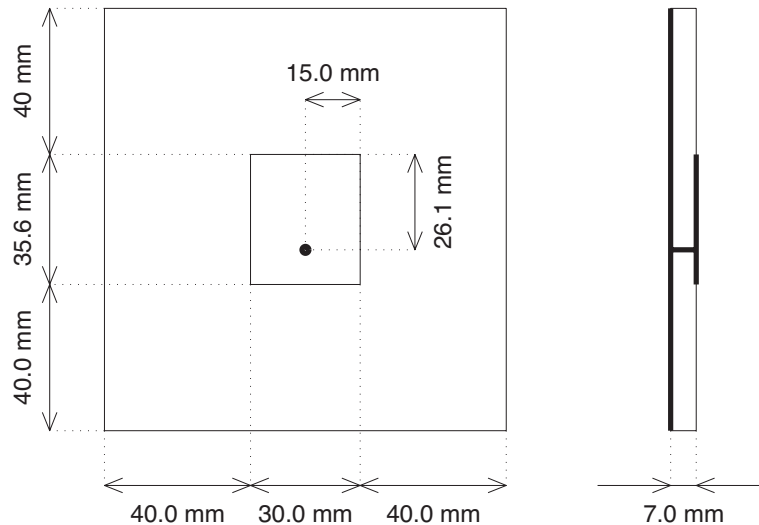
Figure 3: The patch antenna on a finite rectangular ground plane. The view from above and the side are shown to the left and right, respectively, and the position of the feed is shown by the dot in the view from above.

2.3   FDTD computation of radiation patterns

A preliminary study was performed with an FDTD [14, 16, 19] scheme allowing for arbitrary variation in the material parameters together with a simple model of the feeding coaxial cable.

We place the antenna in a simulation box to compute the radiation pattern. The FDTD grid is constructed such that it complies with the ground plane, the slab and the patch. The feed is modeled by defining the electric field, with time dependence as in (2.3) at the edges of the FDTD cells coinciding with the cylinder axis of the inner conductor of the physical coaxial cable. This can also be describded as a time dependent voltage source between the feed point and the ground plane. The radiation pattern is obtained by means of a near-to-far-field (NTF) transformation [16]. We apply an NTF transformation using third order Lagrange interpolation and four point Gauss quadrature [15]. It converges with an $O(h^4)$ error and gives a maximum error of 0.05 % when $\lambda/h = 18$, where h is the cell size. The outward propagating wave is absorbed at the outer boundary by a "sponge layer" [12].

3   Results

In this section, we present results on the bandwidth, radiation efficiency, and radiation patterns for patch antennas on infinite substrates with different spatial variations of the permittivity. The dispersion curves of surface waves for such substrates are also shown. Furthermore, we investigate the influence of finite, inhomogeneous

substrates on the bandwidth.

Here, we refer to bandwidth as the half-power bandwidth $\Delta f/f_0$ for the total radiated power $P_t = 1 - |S_{11}|^2$, where f_0 is the resonant frequency. Furthermore, $\Delta f = f_2 - f_1$ corresponds to the frequency interval $[f_1, f_2]$ where P_t is at least half of the maximum power at f_0. It should be emphasized that the results presented for the hybrid method are computed on one finite grid size and, consequently, the value of, *e.g.*, S_{11}, is subject to some discretization errors. However, the main objective at this point is to find the parameters which have major influence on the bandwidth and it should be safe to compare the FEM-FDTD computations with each other to identify such trends.

3.1 Infinite substrate

In the case of an infinite substrate and an infinite ground plane, we let the permittivity be a function of the height above the ground plane using the profiles shown in Table 1. Here, the constant relative permittivity $\epsilon = 8/3$ corresponds to the homogenized value of the increasing and decreasing reciprocal profiles according to (2.2).

Permittivity profile	$\epsilon(z)$
Constant	$8/3$
Increasing reciprocal	$8/(4 - 2z/d)$
Decreasing reciprocal	$8/(2 + 2z/d)$

Table 1: Permittivity profiles.

The hybrid method was used to compute the reflection coefficient S_{11} for the rectangular patch shown in Figure 3. The Padé approximation (of the computed S_{11}) is shown in Figure 4 by the solid, dashed, and dash-dotted curves for the constant, increasing, and decreasing permittivity profile, respectively. The computed values are shown by circles. We found that the half-power-bandwidth for P_t was 14.4% for the constant profile, 13.8% for the increasing reciprocal profile, and 15.2% for the decreasing reciprocal profile. It is important to notice that the resonance frequencies are slightly different for the three profiles.

The bandwidth of a patch antenna with inhomogeneous substrate has to be compared to the bandwidth of a patch antenna with a homogeneous substrate in order to discover advantages and disadvantages with the inhomogeneous substrate. For a specific profile in Table 1 we compute the bandwidth of a patch antenna with the same geometry and resonance frequency, but with a homogeneous substrate. This can be referred to as numerical homogenization. As reported above, the increasing reciprocal profile gives a half-power-bandwidth of 13.8%. The bandwidth of the corresponding homogeneous patch antenna is 14.4%, *i.e.*, the increasing reciprocal profile lowers the bandwidth by 0.6%. The decreasing reciprocal profile increases the bandwidth by 0.5% since the corresponding homogeneous substrate yields a bandwidth of 14.7%.
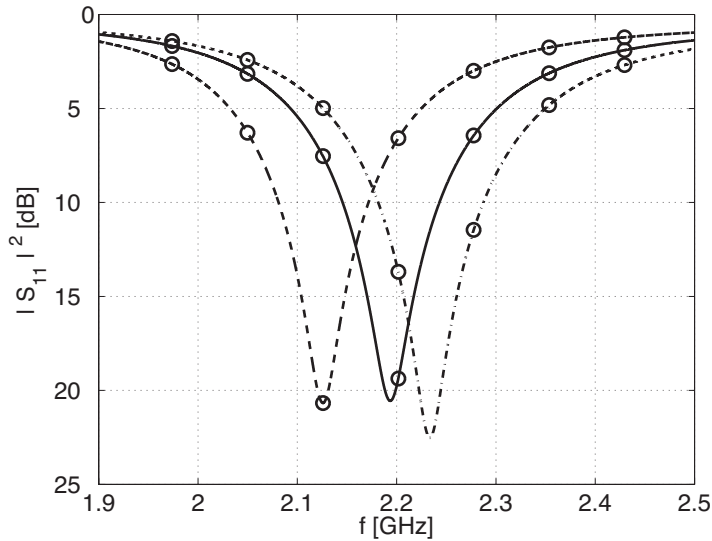
Figure 4: The reflection coefficient S_{11} for the three profiles shown in Table 1 computed by the hybrid method: constant profile – solid curve, increasing reciprocal profile – dashed curve, and decreasing reciprocal profile – dash-dotted curve.

Some of the power P_t are bound to surface waves, i.e. $P_t = P_r + P_{sw}$ where P_r is the radiated power associated with the space wave and P_{sw} is the corresponding power for the surface wave. We have used the analytical model outlined in Section 2.1 to investigate such effects for circular patch antennas on a number of different inhomogeneous substrates [9], including those in Table 1. We found that the ratio P_r/P_{sw} increases with lower values of the homogenized permittivity and thinner substrates. Furthermore, profiles with an increasing permittivity profile gave somewhat higher P_r/P_{sw} compared to the corresponding decreasing profiles.

The dispersion curves of the surface waves for the inhomogeneous substrates in Table 1 were calculated using the analytical model, and they are shown in Figure 5 for the constant (lower figure) and increasing reciprocal (upper figure) permittivity profile. We note that the dispersion curves cross each other for an increasing profile. For the constant and the decreasing permittivity profiles the dispersion curves do not cross one another.

Figure 6 shows the radiation efficiency, defined as $P_r/(P_r + P_{sw})$, by the solid and dashed curves for a circular patch on a substrate with the decreasing reciprocal and the constant permittivity profile shown in Table 1, respectively.

3.2 Finite substrate

For the finite geometry shown in Figure 3, we allow the relative permittivity ϵ of the slab to be a function of x, y and z given by

$$\epsilon = \epsilon_c + \epsilon_\Delta \left[\left(\frac{x - x_0}{\Delta x} \right)^2 + \left(\frac{y - y_0}{\Delta y} \right)^2 + \left(\frac{z - z_0}{\Delta z} \right)^2 \right] \quad (3.1)$$
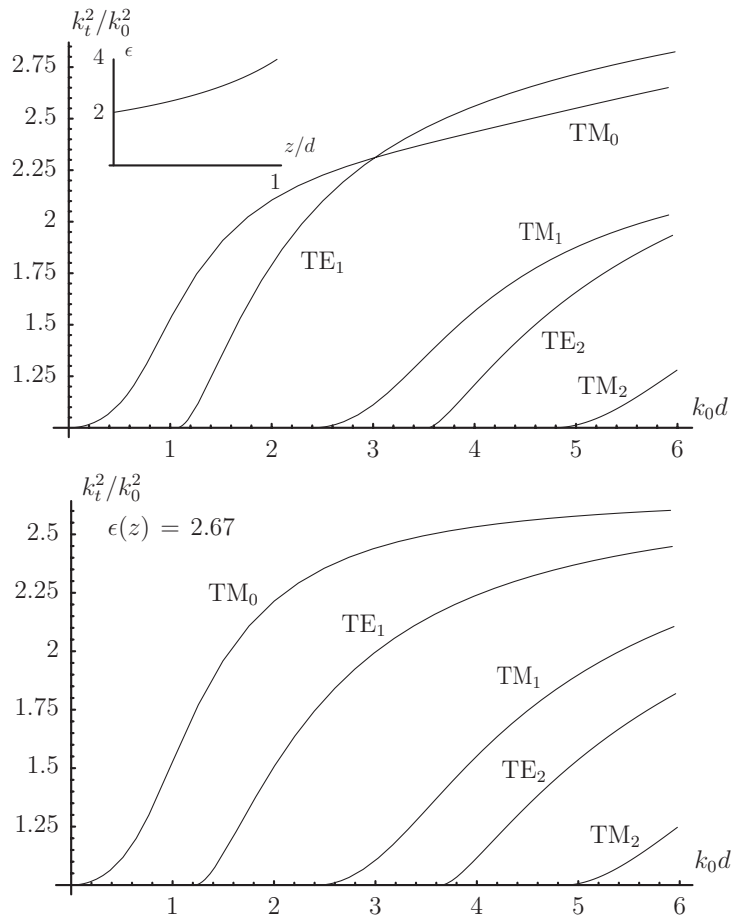
Figure 5: The dispersion curves for the increasing reciprocal and constant permittivity profiles in Table 1 are shown in the upper and lower plot, respectively. The transverse wave number is denoted k_t, d is the thickness of the substrate, and k_0 is the free space wave number.

where we fix $\epsilon_c = \epsilon_\Delta = 2$. Furthermore, we let x_0 and y_0 correspond to the midpoint of the patch. We chose Δx to take the value $l_x/2$, l_x or ∞, and Δy to take the value $l_y/2$, l_y or ∞. Here, $l_x = 30.0$ mm is the width of the patch, *i.e.* perpendicular to the current on the patch, and $l_y = 35.6$ mm is the length of the patch. The parameters z_0 and Δz are given in Table 2. Note that the substrates with the height variation labeled C in Table 2 are identical to turning the corresponding substrates labeled A upside down.

In Figure 7, the half-power bandwidth for P_t is shown in percent as a function of Δx and Δy for the height variation labeled A in Table 2. The corresponding bandwidth is shown in Figure 8 and 9 for profile B and C, respectively. For $l_x/\Delta x = l_y/\Delta y = 0$, the constant relative permittivity $\epsilon = 2$ for profile B does not correspond to the homogenized relative permittivity $\epsilon^{hom} = 8/\pi$ of profile A and C. An additional computation for a homogeneous substrate with $\epsilon^{hom} = 8/\pi$ gave a bandwidth of 14.8%. This confirms the result that a permittivity decreasing with height increases
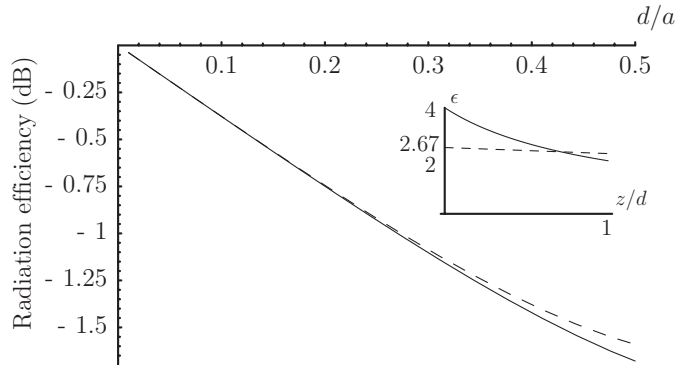
Figure 6: The solid and dashed line show the radiation efficiency for the decreasing reciprocal profile and the constant (homogenized) profile in Table 1, respectively (circular patch).

Permittivity profile	z_0	Δz
A, increasing with z	0	d
B	-	∞
C, decreasing with z	d	d

Table 2: Permittivity profiles.

the bandwidth. Furthermore, Figures 7, 8, and 9 do not indicate any clear advantage of an inhomogeneous substrate. The voltage standing wave ratio (VSWR) is less than 1.6, and the resonant frequency ranges from 1.5 GHz to 2.5 GHz for the profiles presented in Figures 7, 8 and 9.

3.3   Radiation patterns for finite and infinite substrates

Here, we analyze the rectangular patch with finite ground plane, see Figure 3, using FDTD computations for the finite substrate and ground plane. The analytical model described in Section 2.1 is applied to the same patch dimensions, but with an infinite ground plane and substrate. We computed the power gain for a constant permittivity profile using the FDTD scheme with the simple model of the feed and, for comparison, the QuickWave-3D code [4, 7]. QuickWave-3D is based on a generalized Transmission Line Method (TLM) which can treat complex boundaries (by cutting cells) and piecewise constant materials. The constant relative permittivity, $\epsilon = 2.5$, that is used to calculate radiation patterns with FDTD does not correspond to the homogenized relative permittivity $\epsilon^{hom} = 8/3$ of the increasing and decreasing reciprocal profile, see Table 1.

In QuickWave-3D, the feed was modeled as shown in Figure 2 and the coaxial cable was terminated by a port exciting the TEM mode and absorbing the reflected wave. Thus, we can also compute S_{11} of the antenna accurately and this showed that the resonant frequency f_r is 2.37 GHz ($\epsilon = 2.5$). For the FDTD, we used $t_0 = 1/f_r$,
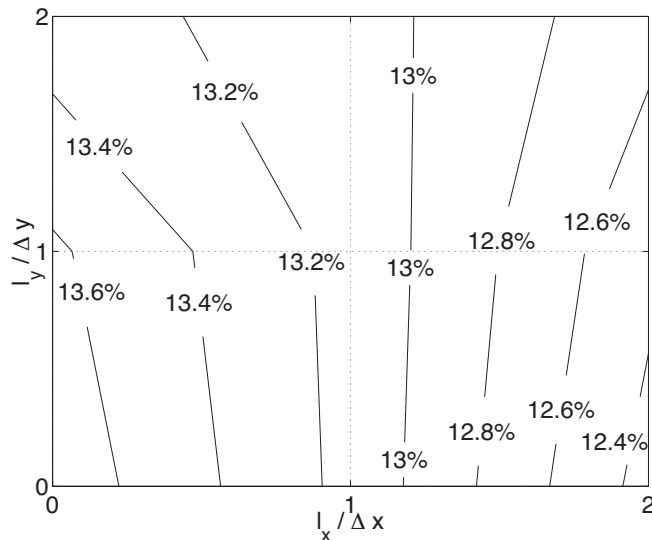
Figure 7: Half-power bandwidth for P_t for profile A in Table 2.

$d_0 = 1/2f_r$, see (2.3). The typical cell size was 2.3 mm. The basic grid of the TLM had the typical cell sizes 1.0 mm, 0.5 mm, and 0.1 mm in the air, the slab, and the coaxial cable, respectively.

The results for the E- and H-plane at f_r are shown in Figure 10 to the left and right, respectively. The dashed and solid curves correspond to the FDTD with a simple feed and QuickWave-3D, respectively. The power gain is normalized by its maximum value over the unit sphere. It should be mentioned that the geometry below the ground plane is not the same for the two schemes. In QuickWave-3D, the coaxial cable extends about 10 mm below the ground plane while it is absent in the FDTD simulation.

In Figures 11 and 12, the power gain in the E- and H-planes are plotted for the increasing and decreasing reciprocal profile, respectively. Results for the theoretical model and the FDTD are shown by dashed and solid curves, respectively. The results from the theoretical model in Figures 11 and 12 are computed for the resonant frequency 2.58 GHz, given by (2.1). The FDTD computations are performed at 2.37 GHz, which is the resonance frequency computed with Quickwave-3D for $\epsilon = 2.5$. It should also be pointed out that small deviations from the true resonance frequency do only have a small influence on the radiation pattern. The radiation patterns, computed with FDTD, presented in Figures 11 and 12 are representative, although they are not computed at the true resonance frequency.

Comparing our FDTD results, the power gain for the decreasing reciprocal profile deviates less than 1 dB, over the complete angle cut, from the corresponding curves for the slab with constant permittivity. In the case of increasing reciprocal profile, the FDTD gives a somewhat higher radiation in general for the back direction and a slightly broader main lobe. The radiation patterns computed with FDTD and the analytic method differ more in the E-plane than in the H-plane. This can be
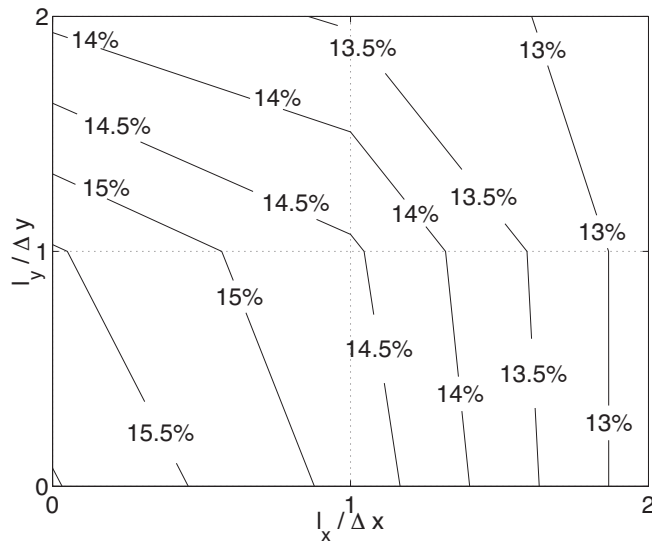
Figure 8: Half-power bandwidth for P_t for profile B in Table 2.

explained by the asymmetry introduced in the E-plane by the feeding point. The analytic method does not take the feeding point into account, and we do not get any back radiation due to the infinite ground plane. From Figure 10, we conclude that the simple feed is a good approximation.

4   Conclusion

We have presented a study on how inhomogeneous substrates for patch antennas influence the performance in terms of surface waves, radiation efficiency, bandwidth, and radiation patterns. It is well known [2] that, for a homogeneous substrate, a higher permittivity gives a more concentrated field below the patch, a lower resonance frequency, and a narrower bandwidth. For inhomogeneous substrates with a *fixed homogenized value* of the permittivity, our results indicate that an increase of the permittivity in the vicinity of the patch lowers the bandwidth and the resonance frequency. To be specific, the FEM-FDTD computations indicate that a permittivity profile which decreases (increases) as a function of height from the ground plane somewhat improves (lowers) the bandwidth compared to a patch antenna of the same size with a homogeneous substrate and the same resonance frequency.

We also see that an increasing (decreasing) permittivity profile yields a lower (higher) resonance frequency than the corresponding homogenized permittivity. Furthermore, the analytical technique shows that inhomogeneous substrates with the permittivity only varying with the height influence the field pattern within the substrate, but not the radiation efficiency.

Comparing our results of the FDTD scheme, the slab with constant permittivity and the decreasing reciprocal profile for the substrate give essentially the same power gain patterns. For the increasing reciprocal profile with a finite ground plane,
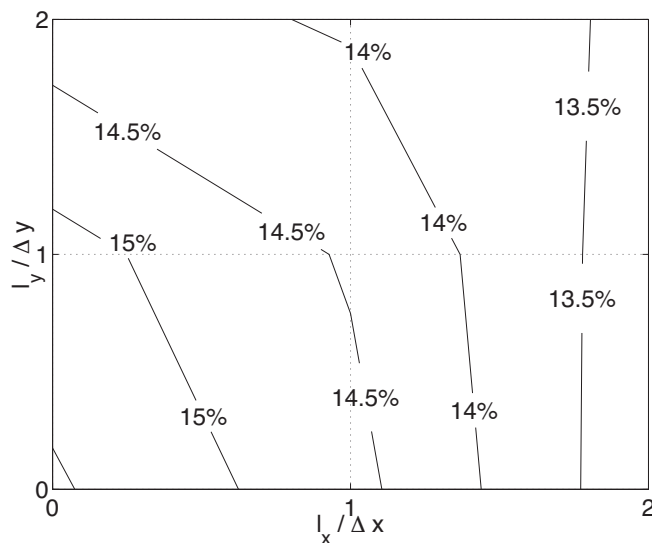
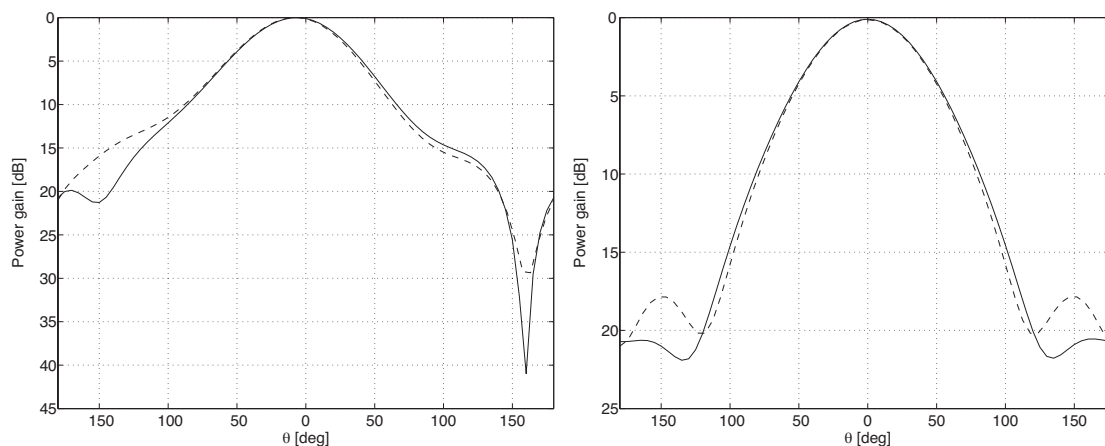**Figure 9**: Half-power bandwidth for P_t for profile C in Table 2.

Figure 10: Power gain in the E-plane (left figure) and H-plane (right figure) for the constant profile with $\epsilon = 2.5$. The dashed and solid curves correspond to the FDTD with a simple feed and QuickWave-3D, respectively.

the radiation in the back direction increases and the main lobe becomes somewhat broader. However, we must conclude that only small influences on the radiation patterns are observed.

References

[1] N. G. Alexopoulos, P. B. Katehi, and D. Rutledge. Substrate optimization for integrated circuit antennas. *IEEE Trans. Microwave Theory Tech.*, **31**(7), 550–557, 1983.
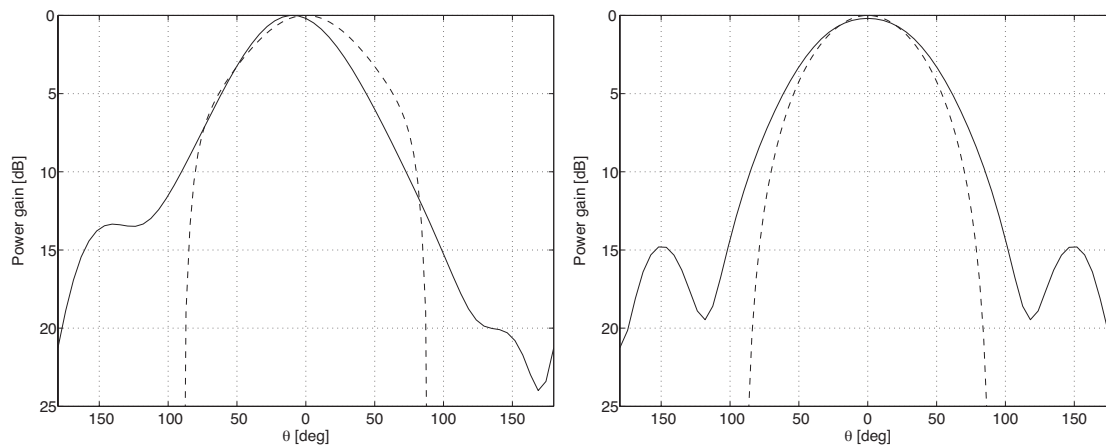
Figure 11: Power gain in the E-plane (left figure) and H-plane (right figure) for the increasing profile. The dashed and solid curves correspond to the analytic calculation and the FDTD with a simple feed, respectively.
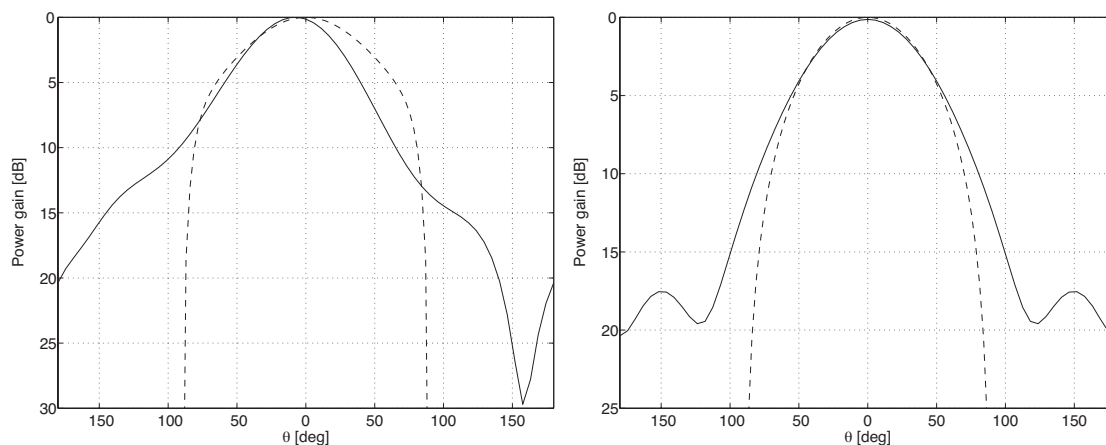

Figure 12: Power gain in the E-plane (left figure) and H-plane (right figure) for the decreasing profile. The dashed and solid curves correspond to the analytic calculation and the FDTD with a simple feed, respectively.

[2] C. A. Balanis. *Antenna Theory*. John Wiley & Sons, New York, second edition, 1997.

[3] S. Balay, W. Gropp, L. C. McInnes, and B. Smith. The portable, extensible toolkit for scientific computation. http://www-fp.mcs.anl.gov/petsc/index.html.

[4] M. Celuch-Marcysiak and W. K. Gwarek. Generalized TLM algorithms with controlled stability margin and their equivalence with finite-difference formulations for modified grids. *IEEE Trans. Microwave Theory Tech.*, **43**(9), 2081–2089, September 1995.

[5] R. Cools. Monomial cubature rules since "Stroud": a compilation – part 2. *J. Comp. Appl. Math.*, **112**(1-2), 21–27, 1999.

[6] R. Cools and P. Rabinowitz. Monomial cubature rules since "Stroud": a compilation. *J. Comp. Appl. Math.*, **48**, 309–326, 1993.

[7] W. K. Gwarek. *QuickWave-3D*. Warsaw University of Technology, 1998. Version 1.6.

[8] G. Kristensson, S. Poulsen, and S. Rikte. Propagators and scattering of electromagnetic waves in planar bianisotropic slabs — an application to frequency selective structures. Technical Report LUTEDX/(TEAT-7099)/1–32/(2001), Lund Institute of Technology, Department of Electroscience, P.O. Box 118, S-221 00 Lund, Sweden, 2001.

[9] G. Kristensson, P. Waller, and A. Derneryd. Radiation efficiency and surface waves for patch antennas on inhomogeneous substrates. Technical Report LUTEDX/(TEAT-7100)/1–48/(2001), Lund Institute of Technology, Department of Electroscience, P.O. Box 118, S-221 00 Lund, Sweden, 2001. http://www.es.lth.se.

[10] C. S. Lee, V. Nalbandian, and F. Schwering. Dual-frequency microstrip antenna with inhomogeneously filled dielectric substrate. *Microwave Opt. Techn. Lett.*, **6**(11), 629–632, 1993.

[11] I. V. Lindell, A. H. Sihvola, S. A. Tretyakov, and A. J. Viitanen. *Electromagnetic Waves in Chiral and Bi-isotropic Media*. Artech House, Boston, London, 1994.

[12] P. G. Petropoulos, L. Zhao, and A. C. Cangellaris. A reflectionless sponge layer absorbing boundary condition for the solution of Maxwell's equations with high-order staggered finite difference schemes. *Journal of Computational Physics*, **139**, 184–208, 1998.

[13] S. Rikte, G. Kristensson, and M. Andersson. Propagation in bianisotropic media—reflection and transmission. *IEE Proc.-H Microwaves, Antennas and Propagation*, **148**(1), 29–36, 2001.

[14] T. Rylander and A. Bondeson. Stable FEM-FDTD hybrid method for Maxwell's equations. *Comput. Phys. Comm.*, **125**, 75–82, March 2000.

[15] T. Rylander and A. Bondeson. Application of stable FEM-FDTD hybrid to scattering problems. *IEEE Trans. Antennas Propagat.*, **50**(2), 141–144, February 2002.

[16] A. Taflove. *Computational electrodynamics: The Finite-Difference Time-Domain Method*. Artech House, Boston, London, 1995.

[17] L. Vegni, F. Bilotti, and A. Toscano. Microstrip disk antennas with inhomogeneous artificial dielectrics. *J. Electro. Waves Applic.*, **14**(9), 1203–1227, 2000.

[18] L. Vegni, F. Bilotti, and A. Toscano. Scattering properties of patch antennas loaded with inhomogeneous substrates via a combined spectral domain-moment method. *Journal of Modern Optics*, **48**(3), 425–438, 2001.

[19] K. S. Yee. Numerical solution of initial boundary value problems involving Maxwell's equations in isotropic media. *IEEE Trans. Antennas Propagat.*, **14**, 302–307, May 1966.

[20] X. F. Zgainski, J. L. Coulomb, and Y. Maréchal. A new family of finite elements: The pyramidal elements. *IEEE Trans. Magnetics*, **32**(3), 1393–1396, May 1996.